Laboratory experiments on nonlinear Rossby adjustment in a channel

Julia Mullarney
Research School of Earth Sciences, Australian National University

1 Introduction and review

Gravity currents in geophysical scenarios such as river outflows or atmospheric boundary layers often occur over sufficiently large scales that they are influenced by the Earth's rotation and therefore behave differently to their non-rotating equivalents. Effects of rotation include lateral mixing, baroclinic instability and the current is deflected to the right (left) in the northern (southern) hemisphere (see Griffiths, 1986, for a review). As the current flows along a boundary (such as a coastline or mountain range) mixing occurs and reduces the density difference between the current and ambient fluid, thus changing its velocity and run out distance.

We focus here on the propagation of rotating *dam-break* gravity currents along a vertical wall. These currents are formed by a finite and instantaneous release of a large volume of fluid into a second fluid of different density and are typically realised in the laboratory by the removal of a barrier between two volumes of fluid. Early laboratory experiments by Stern, Whitehead & Hua (1982) revealed an unsteady bore-like current with a blunt nose from which large eddies were detrained and a thin and approximately laminar 'neck' region behind the nose. The nose velocity decreased with time, and in some experiments the current stagnated and formed a large gyre. Two self-similar solutions of the long-wave equations were found to describe the shape of the current: a thinning 'wedge' solution and a 'bore-like' solution with the front steepening in time. Stern (1980) and Stern *et al.* (1982) also predicted the existence of a *limiting bore*. This bore has the property that its dimensionless upstream width is maximal among all intrusions ($L < 1/\sqrt{2}L_R$, where L is the width and L_R is the Rossby radius of deformation based on the local depth of the nose). Intrusions initiated in wider channels adjust so that a thinner current propagates downstream. It should be noted that the theory developed by Stern *et al.* (1982) is not a complete solution to the dam-break initial value problem and thus the connection of this solution to the dam break problem is unresolved.

An extensive set of experiments by Griffiths & Hopfinger (1983) also showed that the width of the current appeared to asymptote (in this case to $0.6L_R$) directly behind the nose, however further upstream the current is widened by mixing and the width exceeds the

theoretical maximum ($L \approx L_R$ at ten deformation radii upstream of the nose). The currents observed were qualitatively similar to those in Stern *et al.* (1982) and it was shown further that the nose velocity decays exponentially with time. Griffiths & Hopfinger (1983) found that the growth rate of the current billows was much greater than the rotation rate and hence the billows were attributed to a Kelvin-Helmholtz instability and not to a hydrostatic instability as suggested by Stern (1980). Diffusion of momentum by horizontal eddy motions caused broadening of the current upstream of the nose.

We note here that both Stern *et al.* (1982) and Griffiths & Hopfinger (1983) scaled the nose velocity using the local depth of the current which is in contrast to our analysis in which the nose velocity is scaled by the initial layer heights.

Numerical simulations and theoretical analyses of dam-break problems have also revealed interesting features which may have important consequences for the modelling of coastal currents. A weakly nonlinear analysis was developed by Fedorov & Melville (1996) to describe three-dimensional hydraulic jumps propagating along a vertical boundary. A discontinuous solution of the full shallow-water equations was obtained and showed that a shock may exist and it can be felt up to three times further offshore than a regular Kelvin wave. Furthermore, the shock evolves into and maintains a permanent shape which travels at a constant velocity. Far behind the shock the alongshore flow is geostrophic however directly in the lee of the shock there is a region of moderate offshore flow.

Helfrich *et al.* (1999) compared a semi-geostrophic theory (in which geostrophic balance holds in the cross stream but not in the along stream direction) with numerical solution of the two-dimensional shallow water equations. They found a rarefying intrusion (banked along the right hand wall) controlled by the non-dimensional ratio, $\hat{w}$, of the channel width to the Rossby radius of deformation. There is generally good agreement between the two solutions except for in the limit of a wide channel $\hat{w} \gtrsim 2$. In this case the cross channel motions increased and the semigeostrophic assumption becomes invalid. The speeds of the intrusion nose were significantly less in the numerical solution, however this discrepancy was attributed to the finite resolution of the grid being unable to capture the ever thinning nose.

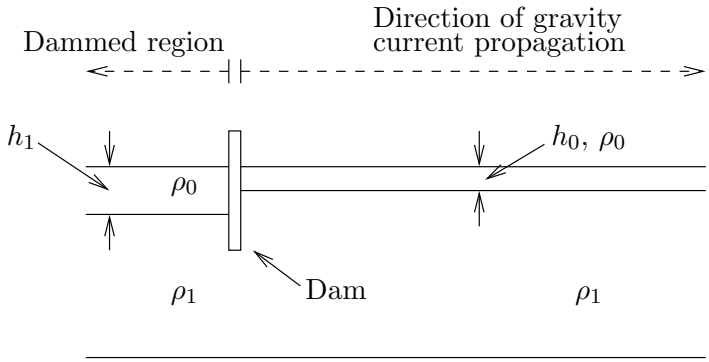

Figure 1: Sketch of two-layer dam break conditions.

If the height of the fluid layer outside of the dammed region is non-zero then the flow gains

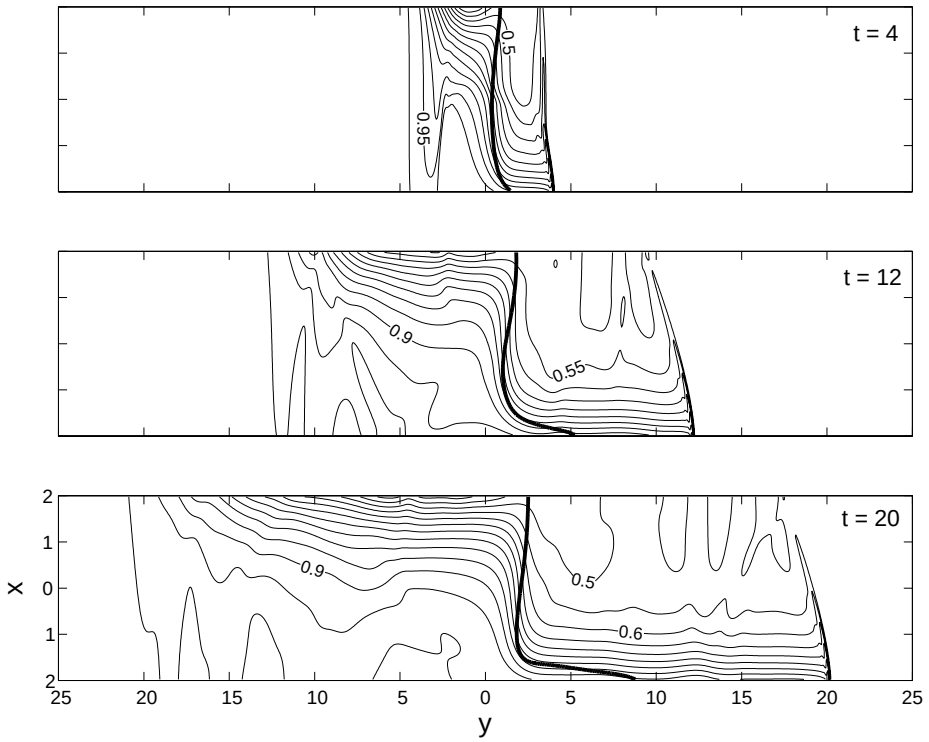

Figure 2: Numerical solution for the non-dimensional depth of the intrusion caused by lifting a dam at $y = 0$. The contour integral is 0.025 and the thicker line is the $c = 0.5$ concentration contour which identifies the interface between the water masses originally upstream and downstream of the dam. In this case $h_0/h_1 = 0.5$ and the ratio of channel width to Rossby deformation radius, $\hat{w} = 4$. For $t = 20$ the potential vorticity front reaches $y \approx 8$, while the leading edge of the shock is located at $y \approx 20$. From Helfrich *et al.* (1999).

much complexity (figure 1). Hermann *et al.* (1989) examined a flow in which the depth difference across the dam was small ($h_1/h_0 \approx 1 + \epsilon$, for $\epsilon \ll 1$). The potential vorticity intrusion propagated down both sides of the channel and for thin channels a small parcel of fluid was ejected from the main boundary current and propagated ahead of the intrusion along the right hand wall. In the case when the depth difference across the dam is not small ($0 < h_1/h_0 < 1$) Helfrich *et al.* (1999) found that the leading rarefying intrusion was replaced by a Kelvin shock. The shock propagated ahead of the potential vorticity front, which appeared again as a rarefying intrusion (figures 2 and 3a). The shock curved across the channel with the angle to the x-axis decreasing with bore amplitude. For small $\hat{w}$ or for small depth difference across the dam the shock attached to both walls; however, as the above quantities increased, it detached from the left hand wall. Behind the shock was a boundary layer of approximately one deformation radius in width, in which the flow was strongly ageostrophic with a large off-shore velocity, figure 3(c) (in agreement with Fedorov & Melville 1996). Potential vorticity was not conserved over the shock and the shock also generated oscillations which Helfrich *et al.* (1999) interpret as Poincaré waves.

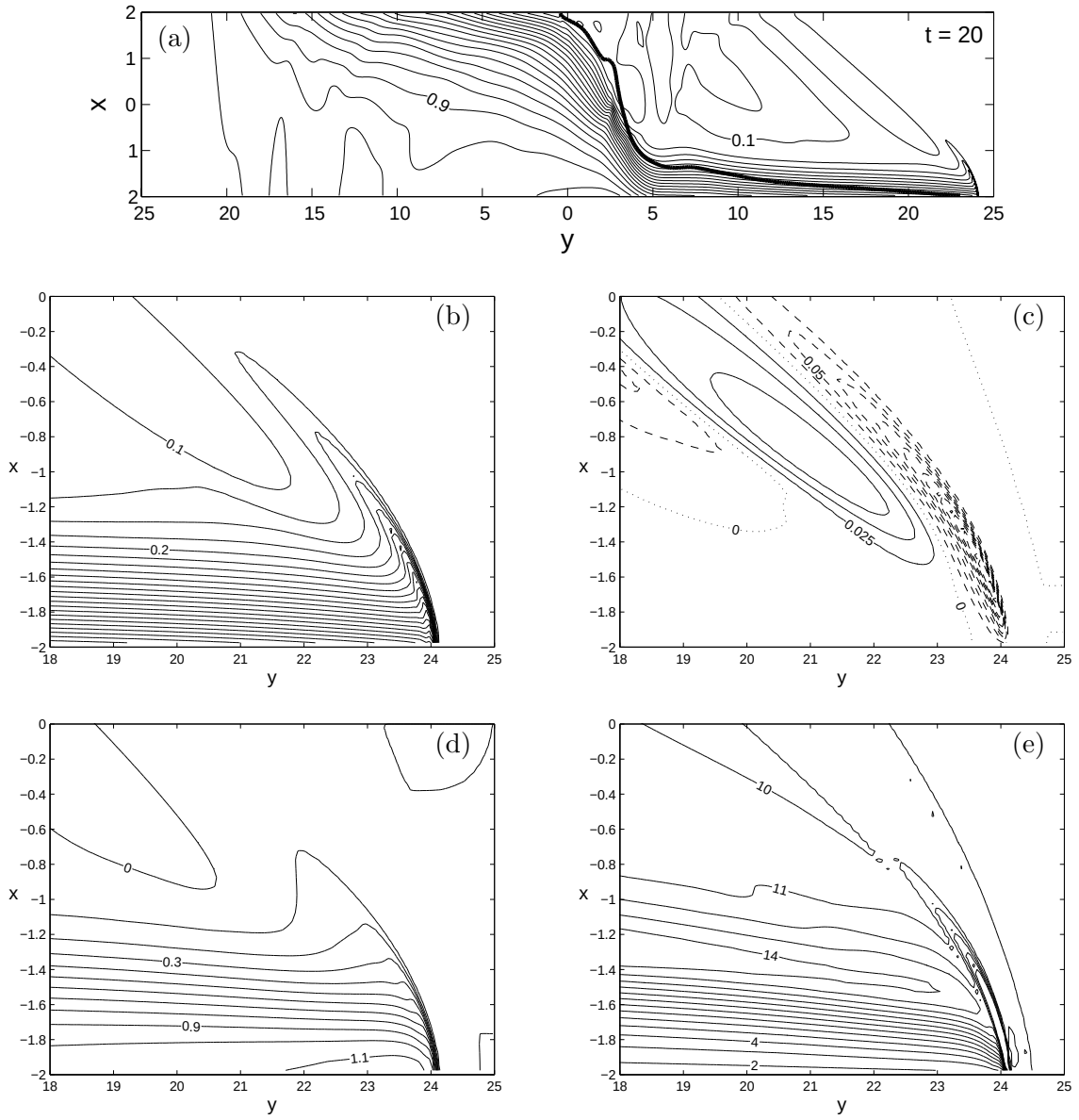

Figure 3: (a) Non-dimensional solution at $t = 20$ as for figure 2, except with $\hat{w} = 4$ and $h_0/h_1 = 0.1$. (b)–(e) show close-up profiles of the bore in (a). Contours plots are of: depth (b), cross-channel velocity u (c), along-channel velocity v (d) and potential vorticity q (e). In (c) solid, dashed and dotted lines correspond to positive, negative and zero velocities, respectively. From Helfrich *et al.* (1999).

A similar representation of the above problem would be the case in which a dam break current flows into a stratified two-layer fluid in which the upper layer is of the same density as the dammed fluid. This situation could arise in a geophysical context with the relaxation of an ocean front (of finite length) after the cessation of wind forcing (Stern & Helfrich, 2002) or when considering the penetration of coastally trapped disturbances into the marine

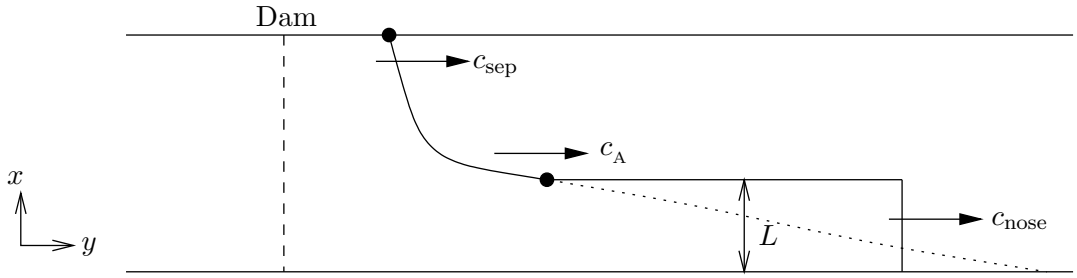

Figure 4: Schematic of the new model. The rarefying gravity current (illustrated by the dotted line) is matched to a bore solution. The attachment point connects the rarefaction and the bore and moves with velocity $C_{\rm A}$.

atmospheric boundary layer (Rogerson, 1999). Stern & Helfrich (2002) extended the study of Helfrich *et al.* (1999) to examine this scenario. The theoretical analysis once again gave an 'expansion' wave (thinning wedge) or a bore solution for the shape of the potential vorticity intrusion. By assuming that the Kelvin shock speed is greater than the speed of the leading potential vorticity intrusion the expansion wave solution was selected. The laboratory experiments of Stern & Helfrich (2002) appear to validate this assumption. The dyed fluid of lower potential vorticity rarefied as it advanced and there were clearly visible instabilities and backward breaking lateral waves at the edge of the current. The Kelvin wave was not directly observable, however its existence was inferred from its effect as it reached the trailing edge of the potential vorticity intrusion. Once the wave had propagated around the full length of the circular tank it displaced the dyed stationary fluid out into the interior and this displaced fluid formed a vortex pair.

2 Aims of this project

New theory developed by Helfrich extends the work of Helfrich *et al.* (1999) and Stern & Helfrich (2002) and aims to describe the evolution of a rarefying gravity current. Both Stern *et al.* (1982) and Griffiths & Hopfinger (1983) used a localised analysis to describe the dynamics at the nose, however their analyses give no information about the current further upstream and in the dammed region. The novel aspect of the new theory is the connection of a rarefaction to a uniform gravity current and uses an explicit bore speed relation of the form $c_b = f(h_b; ...)$, where h_b is the height of the gravity current head. (In particular the choice of $c_b = 1.2\sqrt{g'h_b}$ is supported by Stern *et al.* 1982 and Griffiths & Hopfinger 1983). The present solutions give depth contours of the current for all x and y and the speed of the nose, separation point velocity, attachment point velocity and width of the current as functions of the initial depth of the dammed fluid h_1 and $\hat{w}$ (figure 4). The analytical results agree well with results obtained using a two-layer numerical model.

The present work involves an experimental study for comparison with the above model. The first set of experiments is similar to those conducted by Stern *et al.* (1982) and Griffiths & Hopfinger (1983) and we contrast the three sets of results.

The second set of experiments explores the propagation of a gravity current breaking into a two-layer stratified ambient. Although the experiments are conducted in an annulus they share some similarities with those conducted by Stern & Helfrich (2002). The focus of the study is on the Kelvin bore which propagates ahead of the intrusion of the lower potential vorticity fluid. We aim to obtain a clear direct visualisation of this feature, to measure its velocity and amplitude and to make a comparison with results from Helfrich *et al.* (1999).

3 Experimental set-up

3.1 Apparatus and procedure

The experiments were carried out on in a tank on the 1 m diameter rotating table in the geophysical fluid dynamics laboratory at the Woods Hole Oceanographic Institution. The cylindrical Acrylic tank had an internal diameter and depth of 0.965 m and 0.418 m, respectively. The sides and base of the tank were 10 mm thick. A concentric inner barrier was attached within the tank (by four equally-spaced supports) to form an annulus of width 0.15 m. The inner barrier consisted of a thin clear polycarbonate sheet 0.3 m in depth and was fixed in place 10 mm above the base. This gap at the base of the tank connected the fluid in the inside cylindrical region and the outer annulus to ensure that pressures on either side of the barrier were equal. The water mass in the inner cylinder played no active role in the experiments and its only purpose was to hold the barrier in shape.

A quarter of the annulus was isolated between a fixed vertical end wall and a removable vertical dam to form the dammed region of lower potential vorticity fluid. The end wall and dam also did not reach the base of the tank ensuring the interfaces of the two different fluid regions within the annulus were at identical heights.

The dam was initially left out and the tank was filled with saltwater of density $\rho_2 (> \rho_1)$ to a depth of 27.5 to 30 cm. Densities were measured using an Anton Paar densimeter with an accuracy of 10^{-5}g cm^{-3}. The tank was spun-up counterclockwise at a rate $\Omega = f/2$ until close to solid body rotation. Relatively fresh water of density ρ_1 was then added at the surface until a layer of depth h_0 overlayed the lower denser layer. The fluid was pumped slowly (from source fluid reservoirs attached to the table) through a foam float to minimise mixing.

The tank was allowed to spin-up for a further period of 10–20 minutes before the dam barrier was inserted. Additional source fluid (density ρ_1) was then added to the surface layer in the dammed region until it had reached a depth of h_1. The total depth throughout the tank was H (figure 5). The entire system was brought to near solid body rotation (30 minutes) at which time the experiment was initiated with the removal of the dam. Although the dam was lifted as quickly and smoothly as possible, some unwanted disturbances were created, however their effects dissipated quickly. A summary of all experimental runs is given in table 1.

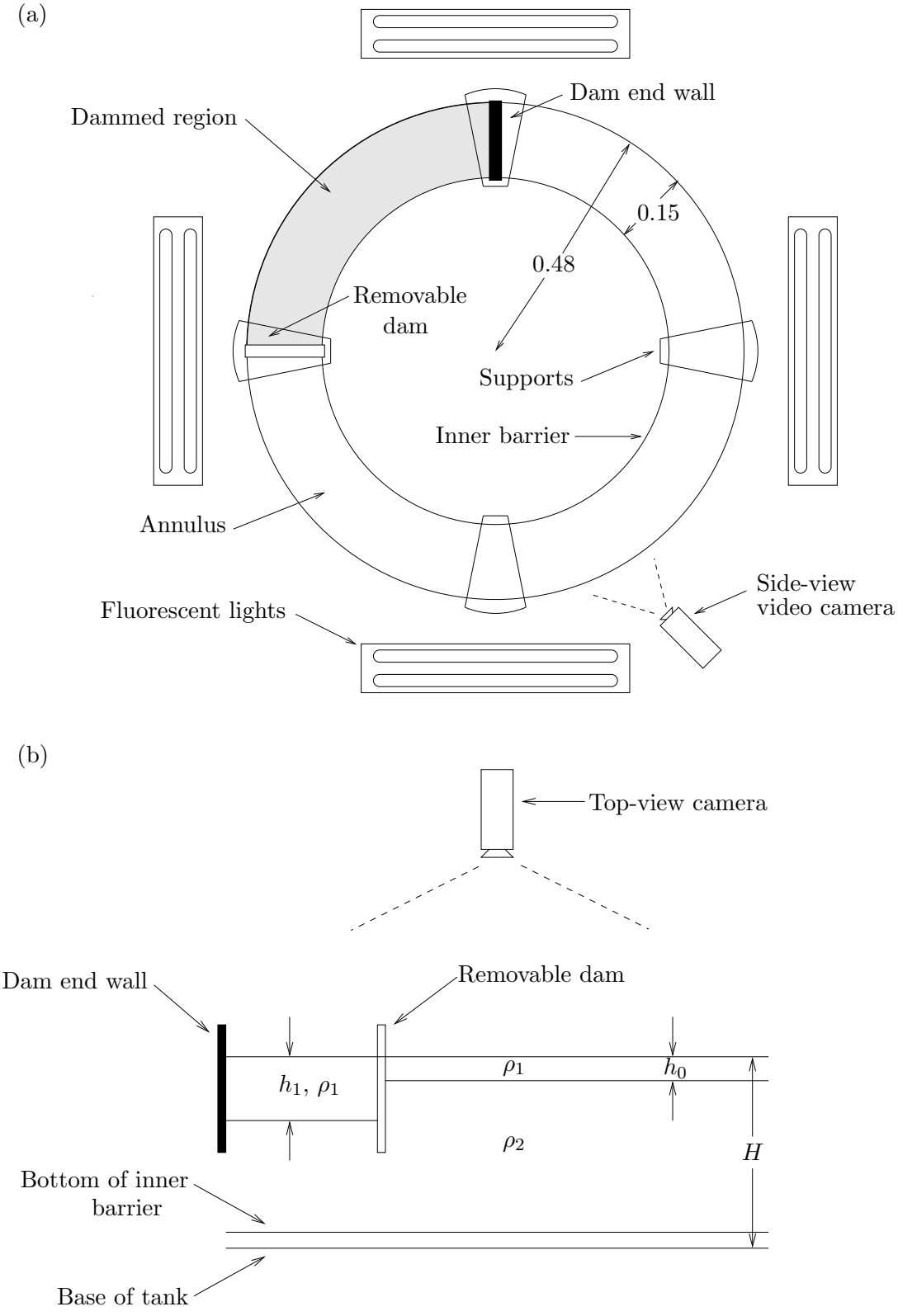

Figure 5: Schematic of experimental apparatus. All lengths are in m. (a) plan view. (b) side view (unwrapped).

Run	h_0	h_1	H	g'	f	h_0/h_1	L_R	$\hat{w}$
1	0	4.5	28.5	5.16	1	0	4.81	3.11
2	0	4.4	28.9	4.95	1.25	0	3.73	4.02
3	0	4.7	28.6	12.56	1	0	7.68	1.95
4	0	4.6	28.5	12.52	0.5	0	15.18	0.99
5	0	5.9	28.8	18.35	0.35	0	29.72	0.50
6	0	6.1	28.8	13.53	0.15	0	60.55	0.25
7	1	4.5	27.5	5.47	1	0.22	4.96	3.02
8	2.8	6	28.7	4.89	1	0.47	5.41	2.77
9	2.2	4.5	28.4	12.47	0.5	0.49	14.98	1.00
10	1.3	4.6	28.9	12.52	0.5	0.28	15.18	0.99
11	3.1	4.1	28.7	12.54	0.5	0.76	14.34	1.05
12	1	3.9	29	5.02	1.25	0.26	3.54	4.24
13	2.2	4.7	28.8	5.01	1.25	0.47	3.88	3.86
14	4.1	5.1	29	5.06	1.25	0.80	4.06	3.69
15	2	6.3	28.4	13.49	0.15	0.32	61.45	0.24
16	2.8	5.4	28.6	13.53	0.15	0.52	56.97	0.26
17	4.5	6	28	13.52	0.15	0.75	60.06	0.25
18	1.7	5.9	29.3	18.39	0.35	0.29	29.76	0.50
19	3.1	6.4	28.5	18.47	0.35	0.48	31.06	0.48
20	4.7	6	29	18.38	0.35	0.78	30.00	0.50
21	1.2	4.4	29	12.53	1	0.27	7.42	2.02
22	2.3	4.8	29.2	12.56	1	0.48	7.77	1.93
23	3	4.4	29.6	12.52	1	0.68	7.42	2.02
24	1.5	5	29.3	5.59	1	0.3	5.29	2.84
25	1.9	4	28.8	5.56	1	0.48	4.71	3.18
26	3.5	4.7	29.9	5.57	1	0.74	5.12	2.93

Table 1: Summary of experimental runs. All parameters are in cgs units. The width of the annulus was 0.15 m in all runs.

3.2 Visualisation

Four sets of (0.585 m long) two-bar fluorescent lights were attached to the table structure. The lights were placed 0.15–0.25 m from the side wall at a height of approximately 0.4 m and were angled slightly down toward the fluid surface. The upper layer of light fluid in front of the dam was usually dyed red and the fluid in the dammed region was dyed blue. After the dam break, the blue fluid therefore marked the position and extent of the potential vorticity intrusion while the propagation of the internal Kelvin wave could be observed by viewing the tank from the side. The wave formed from the lighter red fluid and travelled along the interface between the surface light layer and the denser underlying fluid. The inside edge of the inner boundary was covered with mylar to sharpen the side-view images and to obscure visual effects from the opposite far side of the annulus.

The evolution of the flow after the dam break was monitored by two co-rotating video cameras mounted on the table structure. The plan view was captured by a centred colour camera placed 1.5 m above the surface. The development of the flow at a fixed position with time was captured by a black and white camera mounted on the side of the tank to view a region 0.9–1 m from the dam gate. Over this small region effects of curvature were negligible. Images from both video cameras were digitised and saved directly into a computer at known time intervals (from 1/6 to 2 s). The plan view images were also recorded onto video tape as a back up.

Qualitative images showing the flow at varying positions and time were obtained with a still camera positioned on the floor 2 m from the tank.

4 Results for the experiments with an unstratified fluid ambient ($h_0 = 0$)

4.1 Qualitative description of the flow

The flow behaviour both qualitatively and quantitatively matches that described by Stern *et al.* (1982) and Griffiths & Hopfinger (1983). Figure 6 shows the progress of the current (indicated by the dyed fluid) with time. Immediately after the removal of the dam the released relatively light fluid collapsed forwards and upwards (figure 6a). The fluid collapsed uniformly across the channel until the nose had reached a distance of approximately one Rossby radius of deformation from the dam, at which point the effects of rotation began to be felt by the current and the fluid banked up against the right hand wall (figure 6b). The current propagated as a bore with a blunt bulbous nose which joined to a thin laminar 'neck' region. As described by Stern *et al.* (1982) this neck region was usually the thinnest part of the current. There was some unsteadiness at the edge of the current due to Kelvin-Helmholtz instability and billows were detrained predominantly from the nose but also from further upstream. The unsteadiness and billows were three-dimensional features with much mixing also occurring at the lower edge of the current (figure 7 shows a side view of the current nose).

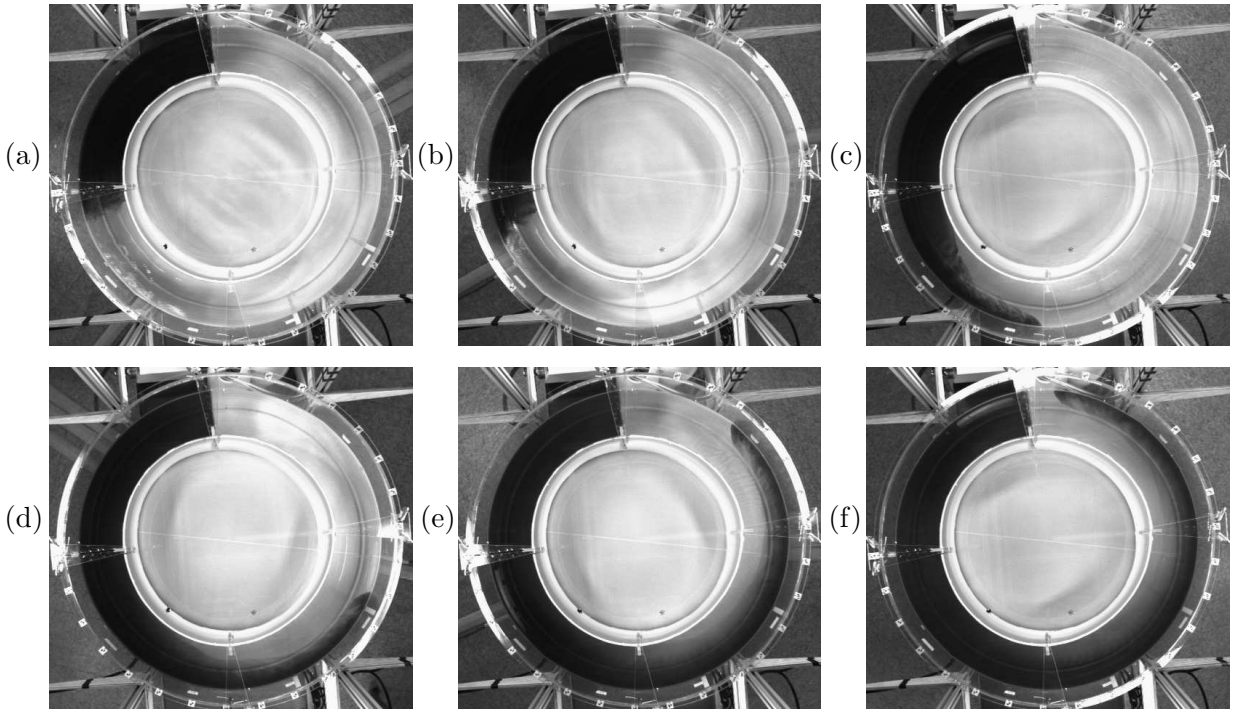

Figure 6: A sequence of photographs from the experiment with $\hat{w} = 0.99$ showing the propagation of the gravity current. The time in seconds after the dam was removed was (a) 2, (b) 3.5, (c) 10, (d) 18, (e) 28, (f) 35.

Although not visible in the photographs, a Kelvin wave formed at the beginning of the experiment. The wave could be seen by looking directly along the dammed region toward the inside back wall of the dam. Immediately after the removal of the dam, the wave of elevation propagated upstream along the interior barrier until it reached the dam end wall, at which point it was reflected around to the outside wall and it continued to propagate downstream behind the nose and in some cases probably caught up with the nose of the current.

In all experiments the digitised images were processed using *Matlab*. Measurements were taken of the position of the nose of the current along the right hand wall and also of the position of the separation point along the left hand wall. The position of the current was plotted as a function of time (with the removal of the dam occurring at $t = 0$) and the results are shown in figure 8. Allowing for an initial adjustment period after the removal of the dam, the velocity remains roughly constant for a period of time and we use a linear fit to this region to give the velocities for comparison with the theoretical predictions. As the current nears the end of the annulus however there is a noticeable decrease in velocity and this departure from the linear fit is more pronounced for larger $\hat{w}$. We hypothesize that lateral friction plays an important role in this decay. In some cases the Kelvin wave which initially propagated upstream catches up with the nose of the current after its reflection off the inside dam wall and this interference may also have an effect on the nose velocity.

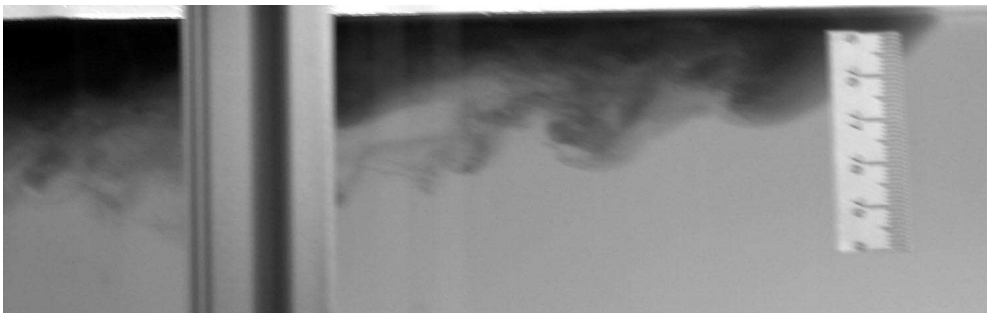

Figure 7: Photograph showing a side view of the current in the experiment with $\hat{w} = 0.99$. Note the unsteadiness and the billows trailing behind the nose. The nose has reached a circumferential distance from the dam of approximately 1 m.

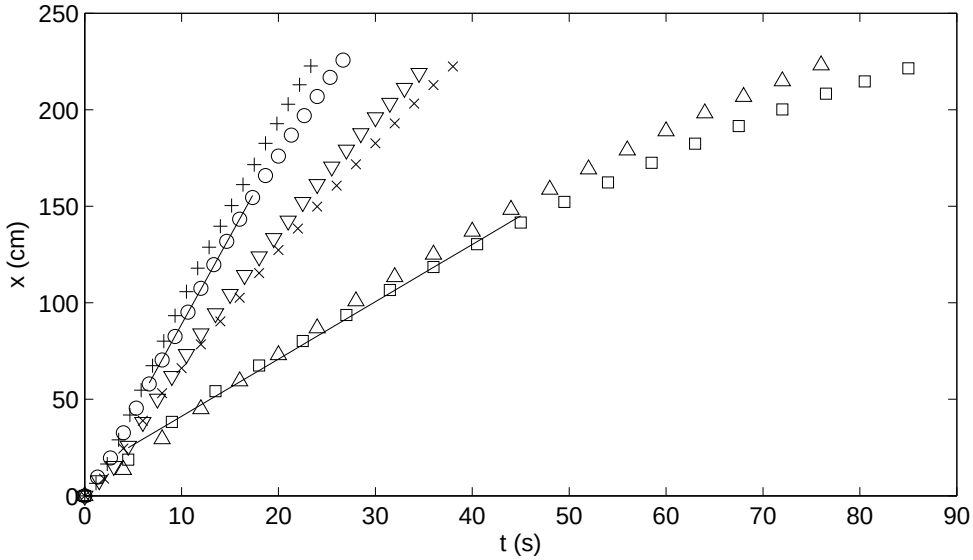

Figure 8: Position of the nose of the current on the outside wall against time. x is the circumferential distance from the dam, which was removed at time $t = 0$. The different symbols are results from experimental runs with parameter $\hat{w} = 0.25\,(+)$, $0.5\,(\bigcirc)$, $0.99\,(\triangledown)$, $1.95\,(\times)$, $3.11\,(\triangle)$, $4.02\,(\square)$. The two solid lines are examples of the linear fit used to determine the velocity of the current.

The width was also measured at each time step. Two definitions of the width were recorded; firstly, the 'vortex sheet' width used by Stern *et al.* (1982) that is, the width from the side wall to the maximum shear line which separates the coherent laminar part of the current from the region of eddies and billows (the darker dyed region in figure 6. Our second definition includes the billows and eddies as part of the current and the width was then the radial distance from their outer edge to the wall. In order to eliminate some of the subjectivity in the measurement process (in both cases), the width was measured at

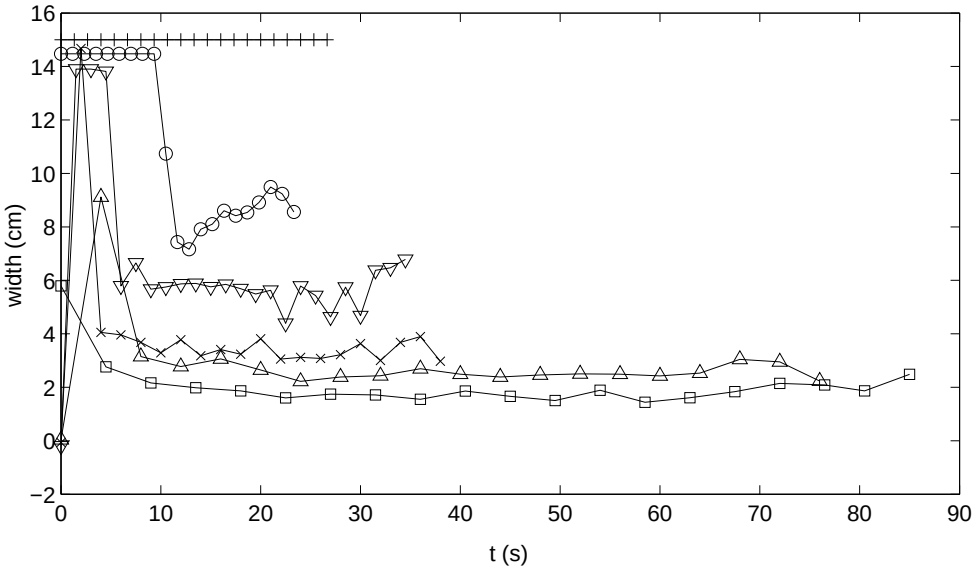

Figure 9: Width of the current against time t for runs with $\hat{w} = 0.25\,(+)$, $0.5\,(\bigcirc)$, $0.99\,(\triangledown)$, $1.95\,(\times)$, $3.11\,(\triangle)$, $4.02\,(\square)$. The dam was removed at time $t = 0$. Here the definition of width includes the billows on the edge of the current.

approximately one Rossby radius of deformation behind the leading edge of the intrusion and, at each time step, five estimates of the edge of the current were made. The mean of these estimates was used as the value for the width at that time step. The width against time graph (figure 9) revealed some initial transience as the fluid slumped followed by a period in which the width of the current remained approximately constant. Here, we use the mean value for each run (neglecting the initial adjustment time) to compare with the numerical and theoretical results found by Helfrich.

The sudden jump in the record for $\hat{w} = 0.5$ indicates that at $t \approx 12\,\mathrm{s}$ the current separated from the interior wall within the region one deformation radius behind the nose. In the run with $\hat{w} = 0.25$ the current width is exactly equal to the width of the channel throughout the experiment, that is the nose and separation point were less that a Rossby radius of deformation apart throughout and in this case the current behaves very similarly to its equivalent (one driven by the same density difference) in a non-rotating frame of reference.

4.2 Comparison with theoretical and numerical predictions

Figure 10 shows theoretical, numerical and experimental results for current width, velocity and height plotted against the governing non-dimensional parameter $\hat{w}$. We also include the results obtained by Stern *et al.* (1982), however these are not in their original form, but have been non-dimensionalised using the initial height of the dammed fluid so as to allow comparison with the present results. Generally there is reasonable agreement between the new results and the theoretical and numerical predictions. The most noticeable discrepancy

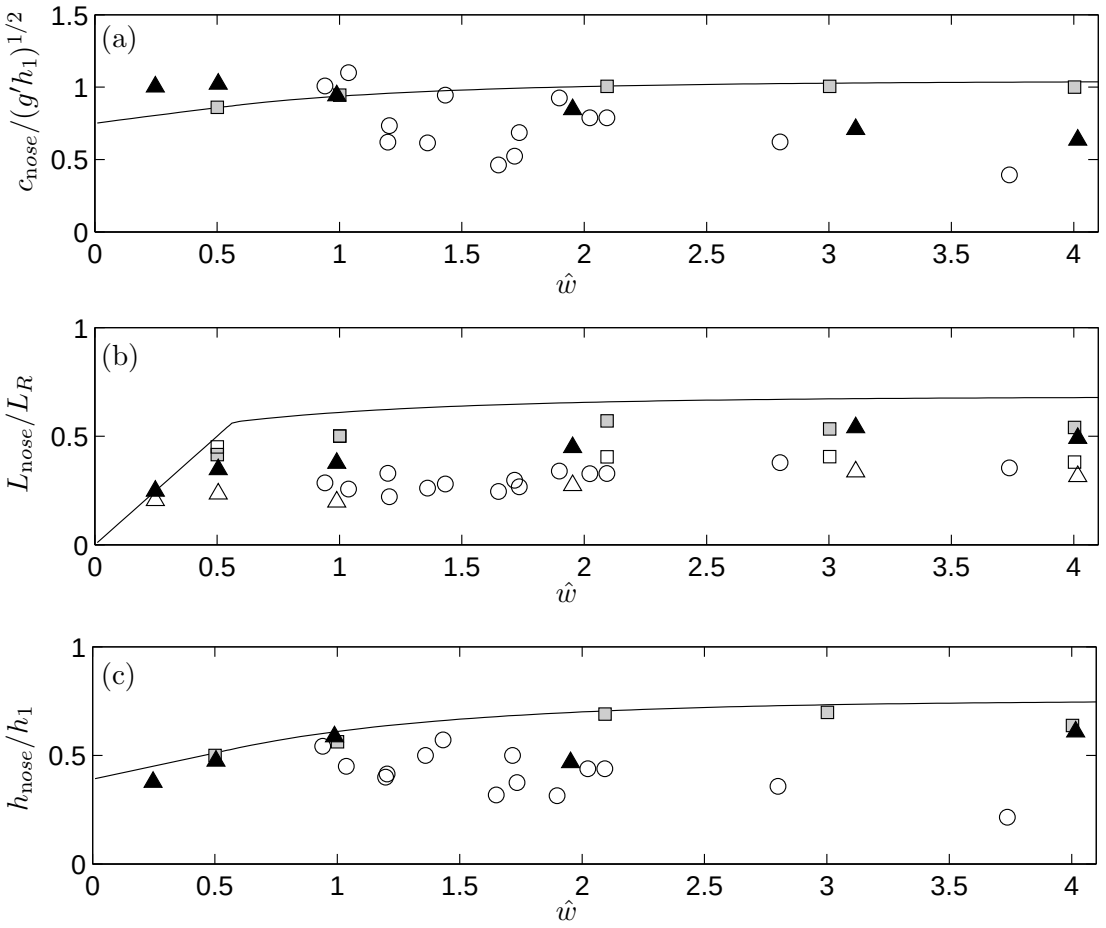

Figure 10: Comparison of the present results for experiments 1–6 (table 1) with previous experimental data (from Stern *et al.*, 1982) and new numerical and theoretical results (from Helfrich). The plots show the current velocity (a), width (b), and height at the nose (c). All results are non-dimensional and plotted against the governing parameter $\hat{w}$. The straight lines are the theoretical results using the bore speed relation $c_{\mathrm{nose}} = 1.2\sqrt{g'h_{\mathrm{b}}}$. The squares are the numerical results, the circles are the results from Stern *et al.* (1982) and the triangles are the results from the present study. In (b) the solid and outline symbols correspond to the two different definitions of width (§ 4.1): the solid symbols include the billows and outline symbols show the width of just the laminar part of the current.

is in the velocity data: the experimental data show a clear decrease for larger $\hat{w}$, whereas the numerical and theoretical data show a very slight increase in nose velocities between $\hat{w} = 1$ and $\hat{w} = 4$.

The theoretical and numerical models do not include all of the physical effects that exist in the experiment and so it is unclear exactly what the discrepancy between the sets of results is due to. Some part can be attributed to the numerical scheme used. The numerical solution points in figure 10 are from the Rutgers ROMS model which is a continuously

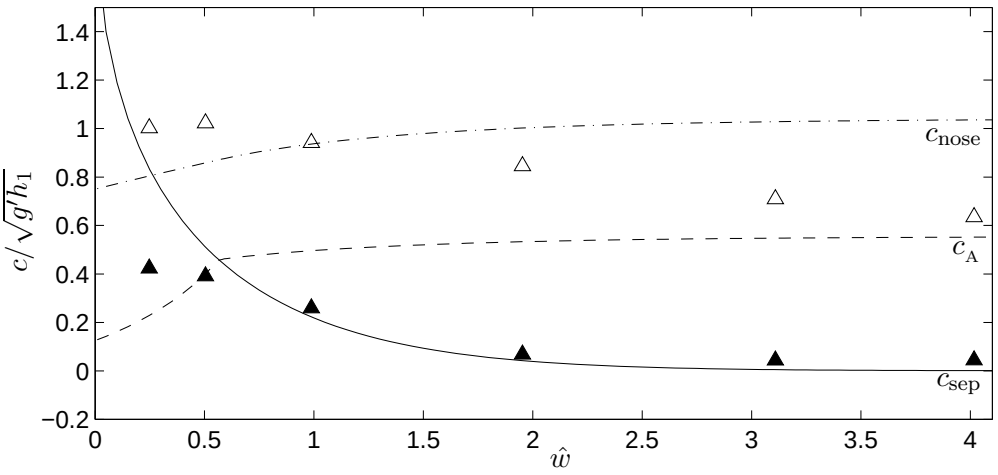

Figure 11: Theoretical and experimental velocities. The lines correspond to theoretical predictions for velocities of the current nose -·-·-, separation point – and attachment point - - (see figure 4). Triangles show experimental results for nose velocity (△) and separation point velocity (▲).

stratified hydrostatic ocean model set up to replicate laboratory scales. It does not include any vertical turbulent mixing sub-model and also uses slip boundaries, so the effects of frictional dissipation are neglected. If this effect were included we would expect the predicted velocities to be lowered, particularly in the cases with larger c_{nose}. The effects of mixing are also neglected in the theoretical and numerical predictions. Mixing would change the value of g' locally at the nose and hence lead to a lower velocity. The finite lower layer may also play a role however these effects are neglected in the theoretical model. Griffiths & Hopfinger (1983) conjecture that cyclonic vortices are generated in the lower layer by turbulence in the current and their experiments show wave and eddy motions exist in the deep lower layer.

The separation point and nose velocities from the present set of experiments are shown in figure 11. The separation point velocities match very well to the theoretical predictions. The agreement is much closer than with the nose velocities. This is probably because the separation point velocities are much slower and hence frictional dissipation plays a much smaller role. There is also less mixing far upstream of the nose in the vicinity of the separation point. We note that in the theoretical results $c_{\mathrm{sep}} < c_A$ for $\hat{w} \lesssim 0.5$, and hence the current is attached across the width of channel to both walls. In this case the separation point velocity should equal the nose velocity ($c_{\mathrm{sep}} \approx c_{\mathrm{nose}}$) however the experimental results do not show a jump between the two curves. However it proved too difficult to measure the attachment point velocity precisely, so this effect could not be studied.

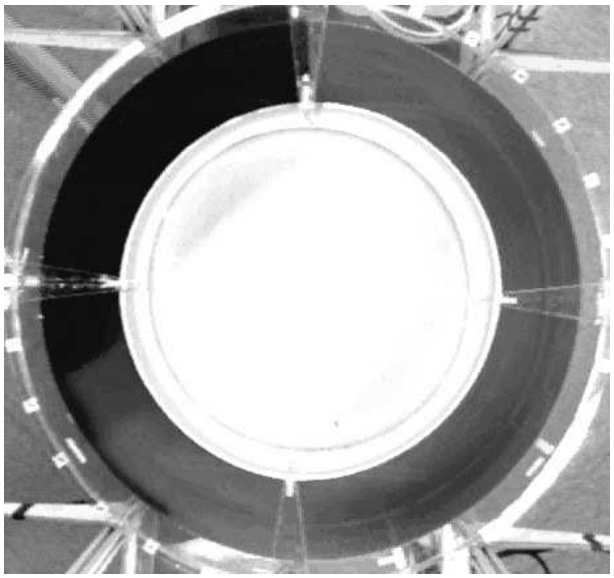

Figure 12: Photograph from the co-rotating camera mounted above the tank in the experiment with $\hat{w} = 1.93$ and $h_0/h_1 = 0.48$. The darker dyed fluid marks the intrusion of lower potential vorticity fluid (which has propagated around $< 1/4$ of the annulus). The Kelvin wave is not seen in this image. The photo was taken approximately 15 s after the removal of the dam.

5 Results for the experiments with a two-layer fluid ambient ($h_0 \neq 0$)

5.1 Qualitative description of the flow

The intrusion of the lower potential vorticity fluid (marked experimentally by the blue dye) propagated as a very thin laminar rarefying front (figure 12) in agreement with the numerical solutions of Helfrich *et al.* (1999). As the experiment progressed the exact position of this intrusion became difficult to see. Thus, in order to estimate the velocity of the nose of the current, its position was plotted against time for the early section of the run when the nose was clearly visible and a linear fit was again used. In the experiments when the depth difference across the dam was small ($h_0/h_1 \approx 0.75$) the current travelled only a short distance (≈ 0.75 m) around the tank before stagnating and forming a large eddy.

There was a disturbance which propagated ahead of, and at a faster velocity than, the potential vorticity intrusion, similar to the shock in the numerical solutions of Helfrich *et al.* (1999). In the experiments this took the form of an undular or a shock-like bore. The series of internal Kelvin waves were clearly visible and propagated along the interface between the lighter red fluid and the clear lower layer. The amplitude of the leading disturbance was the largest with subsequent waves decreasing in size (figure 13). Each time the waves reached an end wall they were reflected off and propagated around the opposite wall of the

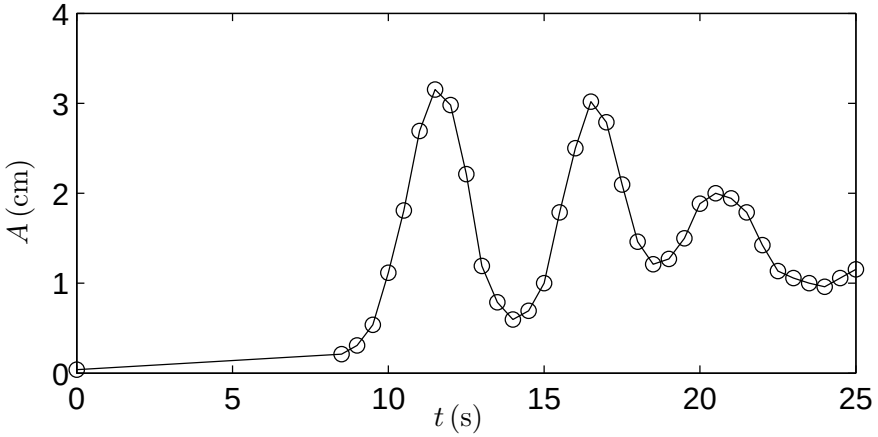

Figure 13: Distortions in the interface measured at a fixed point (∼1 m from the dam) against time from the experiment with $\hat{w} = 0.48$ and $h_0/h_1 = 0.48$. The measurements were taken from images captured by the co-rotating camera mounted on the side of the tank. The data shows the leading internal Kelvin wave and the subsequent chain of smaller waves. The upstream propagation of these waves after reflection off the end wall is not shown here.

annulus in the other direction. Each time a reflection occurred the waves decayed in size however they propagated around the annulus several times before becoming too small to observe. The amplitude of the leading disturbance is plotted in figure 14 and it is found to be proportional to the depth difference across the dam between the two layers of the same density. The reflected bore also affected the advance of the lower potential vorticity fluid (causing the stagnation mentioned above in the cases with $h_0/h_1 \approx 0.75$). As the bore travelled past the potential vorticity front, the front either recoiled or advanced suddenly depending on whether the bore was travelling upstream or downstream, respectively. In many cases a large eddy split off from the current as the bore passed.

For experiments with a large depth difference across the dam $h_0/h_1 \approx 0.25$ the difference between the bore speed and the advancement velocity of the potential vorticity intrusion was small and the two features were almost co-located. In these cases (and those with $h_0/h_1 \approx 0.5$ and $\hat{w} \gtrsim 3$) the bore was turbulent with eddies detraining from the nose (figure 15). For larger values of h_0/h_1 the intrusion of the potential vorticity front was located far behind the leading disturbance which was a much smoother series of waves (figure 16).

5.2 Comparison with theoretical and numerical results

Figure 17 shows the amplitude of the leading bore plotted against the ratio of the initial depths of the layers on either side of the dam. The amplitudes are up to a factor of two larger than in results obtained numerically by Helfrich *et al.* (1999) however the qualitative agreement is good. The amplitude of the leading wave increases as the difference in depths across the dam becomes larger, except when close to the limiting case of $h_0 = 0$ (no layer

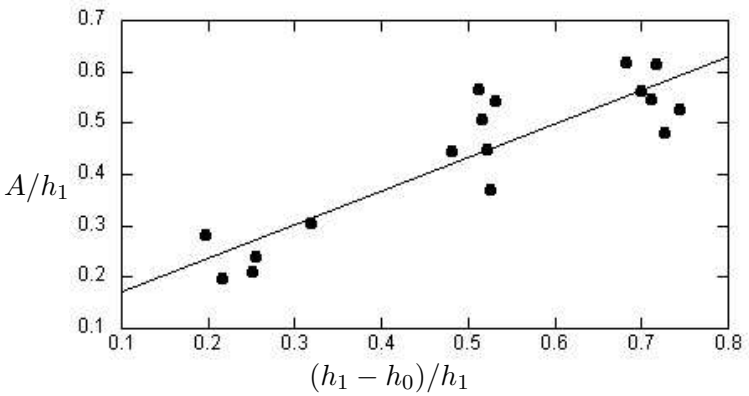

Figure 14: The non-dimensional amplitude A/h_1 of the leading disturbance (measured downward from the interface) against the non-dimensional depth difference across the dam $(h_1 - h_0)/h_1$. The straight line is a linear fit to the data.

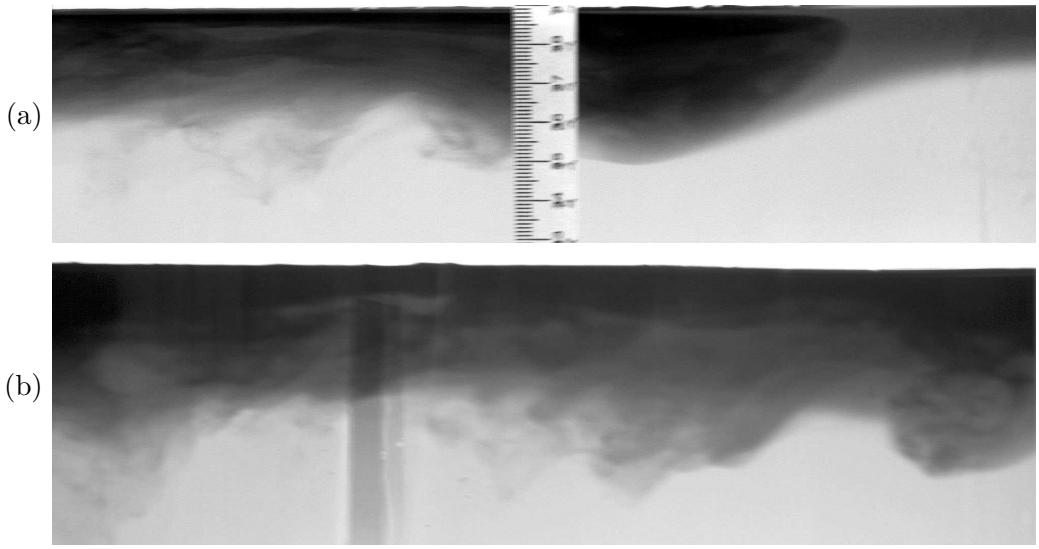

Figure 15: Photographs showing the turbulent structure of the bore from experiments with (a) $\hat{w} = 0.99, h_0/h_1 = 0.28$ and (b) $\hat{w} = 0.5, h_0/h_1 = 0.29$. In both cases the darker fluid marks the fluid of lower potential vorticity. (a) shows the nose of the intrusion (approximately 1/5 from the right hand end of the photo) inside the Kelvin wave. (b) shows the eddying structures just behind the nose of the intrusion.

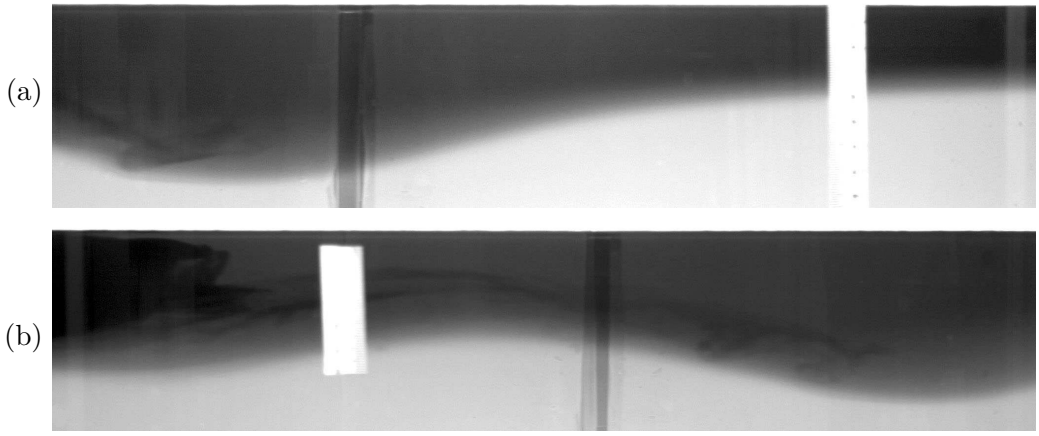

Figure 16: Photographs from the experiment with $\hat{w} = 0.48$ and $h_0/h_1 = 0.48$. (a) shows the leading internal wave and the potential vorticity can just be seen on the left hand side of the photo. (b) shows the smooth shape of the initial and second wave. The white marks are scales on the side of the tank and should be ignored.

of lighter fluid ahead of the dam) and there is a wider range of amplitudes for lower h_0/h_1 across the same range of $\hat{w}$. There is however no clear systematic variation with $\hat{w}$, which is in contrast to the numerical results.

The position of the leading bore was plotted from the sequence of images recorded as it passed into the view of the video camera mounted on the side of the tank. The velocity was then estimated using a linear fit to the data. We note that it is difficult to obtain an accurate estimate over such a short range (particularly for the experiments with $h_0/h_1 \approx 0.75$ in which the wave had a small amplitude) and a better measurement technique is required to allow a careful comparison of results, however the current data are included here for completeness (figure 18). As in the results from § 4.2 the trend indicated in figure 18 is that the velocities are again lower in the experimental case. This is probably attributable to the lack of side wall friction in the numerical model. There is also a large spread in the data and no clear variation with $\hat{w}$.

The velocity of the potential vorticity front was also measured and despite a large scatter matches the numerical data reasonably (figure 19). The agreement is probably better than in the case with $h_0 = 0$ because the current velocities are slower when it propagates into the two-layer ambient and hence there is less frictional dissipation. Also the intrusion rarefies as it advances so mixing is negligible.

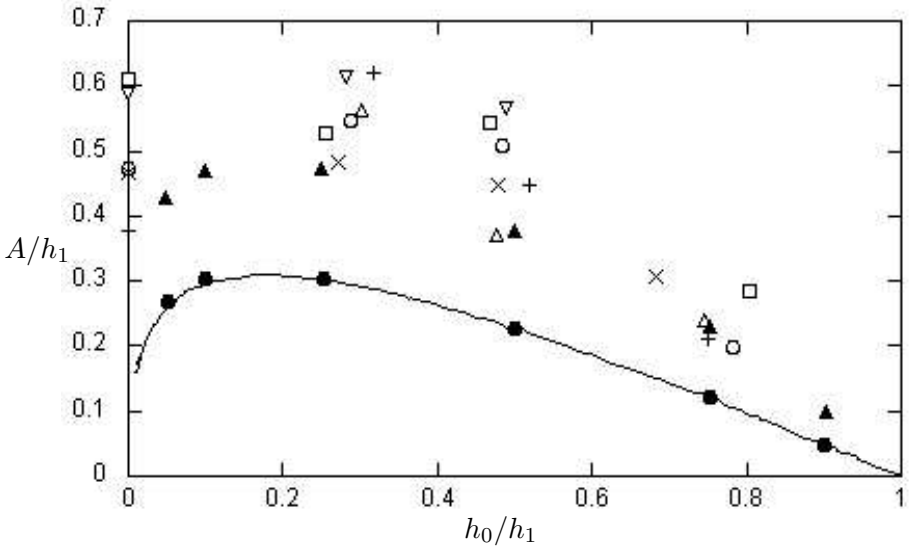

Figure 17: The non-dimensional amplitude of the disturbance against the ratio of depths across the dam. The straight line is the non-rotating theory $\hat{w} = 0$. The solid symbols are the results from Helfrich *et al.* (1999) for $\hat{w}$ =0 (•) and 4 (▲). The outline symbols correspond to the results from the present set of experiments with $\hat{w} = 0.25\,(+)$, $0.5\,(\bigcirc)$, $0.99\,(\triangledown)$, $1.95\,(\times)$, $3.11\,(\triangle)$, $4.02\,(\square)$.

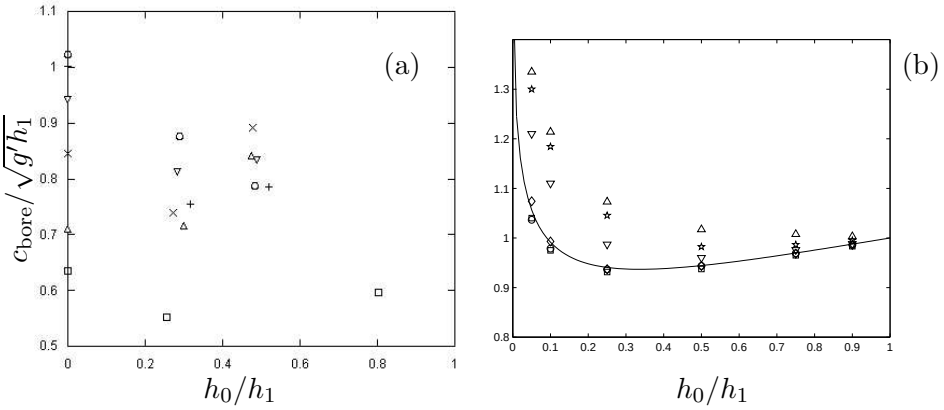

Figure 18: Results showing the bore velocities from (a) the present set of experiments and (b) from Helfrich *et al.* (1999). (a) shows the experiments with $\hat{w} = 0.25\,(+)$, $0.5\,(\bigcirc)$, $0.99\,(\triangledown)$, $1.95\,(\times)$, $3.11\,(\triangle)$, $4.02\,(\square)$. In (b) the velocity increases with $\hat{w}$ from 0 ($\circ$) to 4 ($\triangle$).

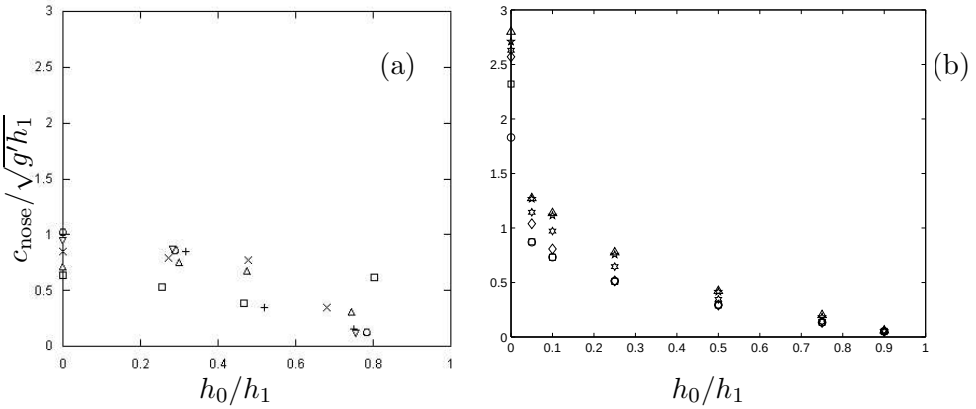

Figure 19: Results showing the velocities of the potential vorticity intrusion from (a) the present set of experiments and (b) from Helfrich *et al.* (1999). (a) shows the experiments with $\hat{w} = 0.25\,(+),\ 0.5\,(\bigcirc),\ 0.99\,(\triangledown),\ 1.95\,(\times),\ 3.11\,(\triangle),\ 4.02\,(\square)$. In (b) the velocity increases with $\hat{w}$ from 0 ($\circ$) to 4 ($\triangle$).

6 Conclusions and further work

We have considered the problem of a dam break gravity current in a rotating frame in two different scenarios. In the first situation we return to the well-studied problem of the current flowing into a uniform ambient. The purpose of the experimental study was a comparison with new theoretical results by Helfrich. The new model connects a bore solution at the nose of the current to a rarefaction solution and relates the height, depth and width of the current to the initial dam conditions. There is good agreement between the theoretical solutions and numerical solutions from a three-dimensional continuously stratified hydrostatic ocean circulation model (set up to imitate laboratory conditions). The laboratory results agree reasonably well with the two sets of results and the differences between them were attributed to viscous effects at the boundaries and mixing, neither of which are present in the models. We note also that small scale turbulence and vertical shear are more significant in the laboratory, so the numerical solutions may be of more use when extrapolating to the oceans.

The second set of experiments considered the case when the ambient fluid outside of the dam region consisted of a two-layer stratification, in which the upper layer of relatively light fluid was of the same density as that released from the dammed region. It was found that a undular bore propagated ahead of the intrusion of fluid of lower potential vorticity. For larger separations between the bore and the potential vorticity front, the bore was a smooth series of waves, whereas when the separation between the potential vorticity front and the bore was small, the bore was turbulent with eddying structures on its lower edge. The amplitude of the leading disturbance was proportional to the initial height difference between the dammed region and the upper layer of the ambient fluid. The preliminary results also show qualitative agreement with numerical results obtained by Helfrich *et al.* (1999) (using a single layer shallow water model).

There are several possible extensions to the work presented here. Both sets of experiments could be repeated in a rectangular tank, which would allow visualisation of the side of the current for a longer time and propagation distance. The set of experiments with the current propagating into the two-layer ambient should be extended over a wider parameter range so a better comparison with the numerical data could be made. The numerical solutions also predict existence of a strong offshore boundary layer directly behind the shock. This feature was not observed in these experiments, possibly it was obscured by the dye in the current. The use of particle tracking in the experiments would give confirmation of whether this flow occurs in the laboratory and enable us to characterise it.

7 Acknowledgements

I'd like to thank Karl Helfrich whose guidance and encouragement made this project possible. All of the numerical and theoretical results are his. Thanks also to Keith Bradley for the amazing help in the lab, to George Veronis for helpful advice and softball coaching, to Neil Balmforth and the staff for letting me attend, to Mountain Dew for the caffeine, and most especially to the other fellows (and pseudo-fellows) for the moral support, Indian cooking and laughs.

References

Fedorov, A. & Melville, W. 1996 Hydraulic jumps at boundaries in rotating fluids. *Journal of Fluid Mechanics* **324**, 55–82.

Griffiths, R. 1986 Gravity currents in rotating systems. *Annual Review of Fluid Mechanics* **18**, 59–86.

Griffiths, R. & Hopfinger, E. 1983 Gravity currents moving along a lateral boundary in a rotating fluid. *Journal of Fluid Mechanics* **134**, 357–399.

Helfrich, K., Huo, A. & Pratt, L. 1999 Nonlinear Rossby adjustment in a channel. *Journal of Fluid Mechanics* **390**, 187–222.

Hermann, A., Rhines, P. & Johnson, E. 1989 Nonlinear Rossby adjustment in a channel: beyond Kelvin waves. *Journal of Fluid Mechanics* **205**, 469–502.

Rogerson, A. 1999 Transcritical flows in the coastal marine atmospheric boundary layer. *Journal of Atmospheric Sciences* **56**, 2761–2779.

Stern, M. 1980 Geostrophic fronts, bores, breaking and blocking waves. *Journal of Fluid Mechanics* **99**, 687–703.

Stern, M. & Helfrich, K. 2002 Propagation of a finite-amplitude potential vorticity front along the wall of a stratified fluid. *Journal of Fluid Mechanics* **468**, 179–204.

Stern, M., Whitehead, J. & Hua, B. 1982 The intrusion of a density current along the coast of a rotating fluid. *Journal of Fluid Mechanics* **123**, 237–265.